JOURNAL OF GEOPHYSICAL RESEARCH, VOL. 106, NO. A9, PAGES 18,981–18,993, SEPTEMBER 1, 2001

# The relationship between suprathermal heavy ion outflow and auroral electron energy deposition: Polar/Ultraviolet Imager and Fast Auroral Snapshot/Time-of-Flight Energy Angle Mass Spectrometer observations

G. R. Wilson and D. M. Ober
Mission Research Corporation, Nashua, New Hampshire

G. A. Germany
Center for Space Plasma and Aeronomic Research, University of Alabama in Huntsville

E. J. Lund
Space Science Center, University of New Hampshire, Durham, New Hampshire

**Abstract.** Ionospheric ions are energized to suprathermal energies (10–1000 eV) in the auroral zone. This produces a much larger quantity of escaping $O^+$ ions than would otherwise occur, given typical ionospheric energies. Until recently, only limited work had been done relating ion upflow characteristics to nearby, contemporaneous auroral forms. We present our results comparing the characteristics of the suprathermal outflowing $O^+$ ions, as measured by the Time-of-Flight Energy Angle Mass Spectrometer instrument on the Fast Auroral Snapshot (FAST) spacecraft, to the auroral forms seen at the foot point of the associated field line, as observed by the Ultraviolet Imager (UVI) on Polar. We present data from FAST nightside auroral zone passes between January 25 and February 11, 1997. During this interval, FAST made ~100 auroral zone passes in the Northern Hemisphere where the aurora was simultaneously imaged by the UVI. Close examination of 50 such passes shows that the regions where suprathermal $O^+$ outflow occurs closely follow the local aurora regardless of how convoluted the auroral forms may be. Taken together, these data show that the flux of escaping $O^+$ ions increases by over a factor of 100 as the auroral intensity in the 1600–1800 Å band increases from 0 to 4 kR. Also, the delay between auroral intensification and saturation $O^+$ flux reaching 3000- to 4000-km altitude is ~5–10 min.

## 1. Introduction

It has long been known that heavy ionospheric ions, such as $O^+$ and $N^+$, can be energized sufficiently to escape from the Earth [*Shelley et al.*, 1972]. The primary region where this occurs is the auroral zone as has been demonstrated by a number of statistical studies that show an overlap between the energetic $O^+$ upflow region and the statistical auroral oval [*Yau et al.*, 1984; *Giles et al.*, 1994]. Additional statistical analysis has demonstrated the dependence of this outflow on season, solar activity, and magnetic activity [*Yau et al.*, 1985a, 1985b]. In particular, it has been shown that $O^+$ outflow increases dramatically with $F10.7$ and $Kp$. Statistical analysis of data from the Ion Composition Experiment (ICE) on the GEOS 1 and 2 satellites has shown that the abundance of $O^+$ in the magnetosphere is similarly dependent on $F10.7$ and $Kp$ [*Young et al.*, 1982].

The ultimate source of the energy that drives heavy ion outflow is the solar wind, which delivers energy to the auroral ionosphere in the form of precipitating energetic electrons or ions, currents, or low-frequency waves. The means by which the energy is finally given to the ions includes frictional heating, centrifugal acceleration, acceleration by parallel potential drops, and perpendicular energization by one of various plasma wave modes (see review by *André and Yau* [1997]). Regardless of what other processes are involved, the escape of heavy ions from Earth's gravity undoubtedly requires either parallel acceleration or perpendicular heating to gain the 10 eV or more of energy needed. In the low-altitude region pertinent to this study (≤ 4000 km), conic distributions dominate over beams [*Gorney et al.*, 1981; *Miyake et al.*, 1996], so that perpendicular heating is the most important process. Recent statistical studies using Freja data at 1700 km [*Norqvist et al.*, 1998] and Fast Auroral Snapshot (FAST) data between 2000 and 4000 km [*Lund et al.*, 2000] suggest that broadband extremely low frequency (BBELF) waves are the dominant heating agent in this region, eclipsing electromagnetic ion cyclotron waves and lower hybrid waves.

Since ion heating is tied to energy inflow to the auroral zone, processes which change the energy input (e.g., substorms) will likely affect the ion outflow rate or location. *Øieroset et al.* [1999] showed, using Viking data, that the outflow rate and the latitudinal extent of the region of energetic ion (40 eV to 1.2 keV) outflow on the dayside increase



Paper number 2000JA000434.
0148-0227/01/2000JA000434$09.00

dramatically with increasing *AE*. *Daglis et al.* [1994] showed, using Active Magnetospheric Particle Tracer Explorer (AMPTE)/CCE charge-energy-mass (CHEM) data (1 to 300 $keVe^{-1}$), that the energy density of the $O^+$ ions in the plasma sheet is well correlated with *AE* during the expansion phase of a substorm. For solar wind origin ions (i.e., $He^{++}$) observed in the plasma sheet, there is little correlation with *AE*. Taken together, these two studies strongly suggest that the outflow of energetic ions from the ionosphere to the plasma sheet responds quickly to changes in energy input.

The ion outflow process is quite complicated, and unraveling the important aspects of it is difficult. It involves a number of different energization processes acting, likely, over a large range of temporal and spatial scales. Although ion heating may begin quickly once energy deposition begins, the change in ion characteristics at some distant point will be delayed by at least the travel time connecting the two points, if not by the timescales over which the ionosphere is modified. Progress in this field has been hampered by the same basic problem that affects most of space physics: Observations from a single spacecraft cannot resolve spatial and temporal ambiguities. If ion upflow data are provided by a single spacecraft, then all that is known are the ion characteristics and ambient environmental characteristics (energetic particles, plasma waves, etc.) on the given field line at the time it is crossed. What is not known are the conditions on the field line before it was crossed. Furthermore, there is no way of knowing what processes or conditions were experienced by the observed ions as they traveled to the spacecraft. This is especially true if the ions convected large distances across field lines to get to the observation point.

Two methods have been employed to try to deal with this problem. One is to use global measures of activity such as *F*10.7, *Kp*, or *AE* to determine ionospheric or auroral zone conditions prior to the time of observation. Such studies have revealed many important aspects of the ion outflow problem, but they lack sufficient spatial resolution to reveal what is happening in the local region where a specific outflow observation is made. Another approach is to use data from multiple spacecraft such as was done by *Peterson et al.* [1993] or *Wilson and Craven* [1999] to determine the conditions at two different altitudes along a field line where ion outflow occurs. Although such observations can reveal many important clues to the overall problem, the requisite spacecraft conjunctions are rather rare.

Another approach that has not been used much is to exploit auroral imaging. Such data can reveal the conditions of the auroral zone both globally and locally and give a measure of energy input to the ionosphere. Sequences of images can give the time history of conditions prior to an outflow observation. This approach was used as part of a study of two ion outflow cases by *Hirahara et al.* [1998]. In addition to the use of other in situ data, ion outflow characteristics observed by the Polar Thermal Ion Dynamics Experiment (TIDE) were compared to auroral conditions at the foot of the field line as observed by the Polar Ultraviolet Imager (UVI). Because the observations were made during the perigee portion of the Polar orbit, the length of time over which the pertinent portion of the aurora was viewed was limited. In the work of *Stevenson et al.* [2000] this basic approach was applied to a number of dayside and nightside auroral zone crossings, and it was found that regions of bright aurora often have large fluxes of upflowing $O^+$ ions.

In this paper we describe analysis of ion outflow as observed by the Time-of-Flight Energy Angle Mass Spectrograph (TEAMS) instrument on the Fast Auroral Snapshot (FAST) explorer spacecraft compared to auroral forms seen by the Ultraviolet Imager (UVI) on the Polar spacecraft. During each 18-hour orbit, Polar is beyond a geocentric distance of 6 $R_E$ for 12 hours. At this distance the 8° field of view of the UVI will see most or all of the auroral zone. With an orbital period of ~2 hours, FAST will fly through the auroral zone five to six times during the interval when the UVI images the auroral zone. In other words, the combination of these two data sets can provide many opportunities to study ion upflow observed in the 2500- to 4000-km altitude range in a context where the current and time history of local energy input to the ionosphere is known. In the present study we have just begun to mine these rich data sets.

## 2. Data Description

The TEAMS instrument on FAST [*Möbius et al.*, 1998] is able to separate ions by arrival angle, energy per charge, and mass per charge. The front end of the instrument is a torodial top hat type electrostatic analyzer (ESA) with a 360° × 8° field of view. It is mounted on the spacecraft so that it will sweep out a full $4\pi$ sr in half of a spacecraft spin. Behind the ESA, ions are accelerated up to 25 kV and sent through a time-of-flight section for mass discrimination. The instrument has an energy range of 3 eV to 12 keV, can readily identify the major ion species ($H^+$, $He^{++}$, $He^+$, $O^+$, and molecular ions), and has a time resolution of 2.5 s. Its angular resolution is 22.5° × 22.5°. Like many particle detectors the TEAMS instrument gradually loses sensitivity over time as its microchannel plates are exposed to increasing larger particle doses. To compare flux measurements directly requires that they be made within a short time interval of each other or that measurements be corrected for the loss in sensitivity.

The TEAMS instrument operated in modes that returned data with different time resolutions. Most of the TEAMS data we used in this study had a 5-s time resolution. In all of our passes the instrument would start in a mode where it sampled every 20 s, and then as it approached the auroral zone, it switched to the 5-s mode. So nearly every TEAMS data sample we use that is taken over the auroral zone is at 5-s resolution. Some of the data at subauroral latitudes were of the 20-s variety.

In this study we use exclusively $O^+$ data taken at altitudes above 2500 km. We do not process the data in any way to remove ram effects or the effects of spacecraft potential. To mitigate these effects, we restrict our attention to ions whose energy exceeds 8 eV. (We do not use a higher energy cutoff, since we want to include as much of the escape flux as possible.) Given the spacecraft velocity, the ram energy of $O^+$ between 2500- and 4000-km altitude is ≤ 4 eV. A review of six months (December 1996 to February 1997 and June 1997 to August 1997) of spacecraft potential measurements made by the Polar electric field instrument near perigee (5000- to 7000-km altitude) indicates that Polar rarely exceed 5 V positive in this region. Given the lower altitude of the FAST spacecraft, it is unlikely that its potential will often exceed 3 V positive.

The integrations over the angle and energy array performed to find the $O^+$ parallel flux were carried out in several steps in order to eliminate or reduce the contribution of precipitating

particle fluxes to the calculation. The energy-pitch angle space sampled by the instrument was divided up into several regions. The first is from 8 eV to 1 keV for all pitch angles outside of the loss and source cones. This is a symmetric integration about a pitch angle of 90° that should, on average, cause the contributions of any precipitating particle that mirror below the spacecraft to cancel out. The second region is from 8 eV to the instrument cutoff energy for the source cone only and adds in the contribution of any upflowing beams. The third region is from 1 keV to the instrument cutoff energy for all pitch angles outside of the source and loss cones. This is the high-energy analog to the first region. The integration over this region is only added to the total if an inspection of the summary data spectrograms reveals that the upflowing $O^+$ conic extends significantly above 1 keV in energy. It is not routinely added in, because the lower count levels typical in this region do not guarantee cancellation by upgoing and downgoing precipitating particle fluxes, and it is a region where contributions from precipitating particles can dominate.

Since the loss cone is typically 25°–30° in the altitude region of interest, the 22.5° angular resolution of the TEAMS instrument may affect the velocity space integrations depending on whether or not a particular measurement pixel is inside or outside of the integration region. We have done several tests to show that this effect does not influence our results at all. We took the 19 passes used for Figures 3 and 4 and redid the velocity space integration so that it covered all pitch angles outside of the loss cone. In effect, we added the high-energy conic region in all of the passes and not just some of them. The change in the fitting parameters and correlation coefficients was insignificant with the largest being ~2%. The retention of a pitch angle boundary at the loss cone will not have an effect, because there are no significant fluxes in this portion of velocity space for the passes used.

The Polar Ultraviolet Imager [*Torr et al.*, 1995] operates in the far ultraviolet (1200–1800 Å) so that it is able to view the sunlit portion of the aurora. It has a circular field of view of 8° with an angular resolution of 0.04°. From apogee this gives a spatial resolution of 30 km. Images are made in four bands centered at 1304, 1356, 1490, and 1700 Å with bandwidths of 50, 70, 175, and 180 Å, respectively. The last two of these filters respond primarily to molecular nitrogen Lyman-Birge-Hopfield (LBH) emissions and are referred to as the LBH-short (LBHs) and LBH-long (LBHl) filters. All of the data used in this paper were from images taken with the LBHl filter. These were flat field corrected and converted into absolute radiance units (kilorayleighs) and they had instrument background removed. No effort was made to remove dayglow, which should have little effect on emission intensities from wintertime, nightside aurora. During all of the passes used, the UVI was operating in a mode where it would take two exposures with the LBHs filter (18 and 37 s), followed by two exposures using the LBHl filter (18 and 37 s, both of which are used), followed by a background reading. The overall timing of the imaging sequence was designed so that the time interval between successive images of the same type was fixed at 3 min 4 s. Because of this, the time spacing between consecutive LBHl images can be as short as 37 s or as long as 147 s. Passes with significant numbers of missing images were not used.

After Polar was placed in orbit, it was discovered that the spacecraft was not balanced properly, resulting in a slight wobble with the same 6-s period as that of the spacecraft spin. For the UVI this results in a reduction of the spatial resolution, in one dimension, from 30 to 300 km. With an average FAST velocity of 6 $kms^{-1}$, and in the worst case where the satellite's ground track parallels the pixel's long dimension, we end up comparing 20 TEAMS flux measurements (one sample every 5 s mapped to 100-km altitude) with one UVI pixel intensity. If we assume a strong correlation between the $O^+$ fluxes and the foot point auroral intensities, then this smearing will not mask this relationship in auroral regions that are relatively uniform. In highly structured regions it will tend to mask the relationship because various oxygen fluxes will be assigned to the same, average auroral intensity. The correlation that we see between these two quantities may therefore be understating the full range of the correlation.

## 3. Examples

In this section we present a few examples of the type of data we are using in this study. The first event occurred on January 28, 1997, between 2040 and 2110 UT. On this date the $F10.7$ index had a value of 71 ($\times 10^{-22}$ W $m^{-2}$ $Hz^{-1}$). At this time of the day, *Kp* went from 4+ to 4-. *Dst* was –43 nT, indicating that a small magnetic storm was in progress. The conditions are then solar minimum, winter, with a moderate level of magnetic activity.

In this pass the magnetic ground track (position of the satellite mapped to 100-km altitude using the International Geomagnetic Reference Field (IGRF) magnetic field model) of FAST passed over eastern Scandinavia and the Kola Peninsula. Plate 1 shows six consecutive images taken with the LBHl filter, plotted in a magnetic latitude and magnetic local time (MLT) coordinate system. Also shown are the FAST ground track and the position of the spacecraft along that track at the time of the image.

The main auroral ban in the UVI images in Plate 1 extended from southern Greenland, across Iceland, and over northern Scandinavia. The small black squares in each image indicate the location of several ground magnetometers. The northernmost is Ny Ålesund (NAL; 78.9°, 12.0°), followed by Bear Island (BJN; 74.5°, 19.2°). (The parenthetical information gives the stations international code and its geographic latitude and longitude.) The southernmost is Nurmijärvi (NUR; 60.5°, 24.7°). The three stations nearly in an east-west line are (from the west) Andenes (AND; 69.3°, 16.0°), Kevo (KEV; 69.8°, 27.0°), and Lovozero (LOZ; 68.0°, 35.1°). These three stations are on or very near the northern coast of Scandinavia.

The portion of the auroral zone that is north of Scandinavia was relatively quiet, compared to the aurora to the west, for many minutes prior to 2059 UT. Some time between 2059 and 2102 UT the electron flux into the auroral zone in this region increased. The timing and location are confirmed from ground-based magnetometers of the International Monitor for Auroral Geomagnetic Effects (IMAGE) network [*Viljanen and Häkkinen*, 1997]. The magnetometer stations at Andenes, Kevo, and Lovozero had similar, large positive $x$ component deflections (220 – 280 nT) that began ~2–4 min before peaking at 2100 UT. The Bear Island station was north of the auroral activation region and had a negative (as opposed to positive) $x$ component deflection of 160 nT that also peaked at 2100 UT. Stations far to the north (NAL) or south (NUR) of

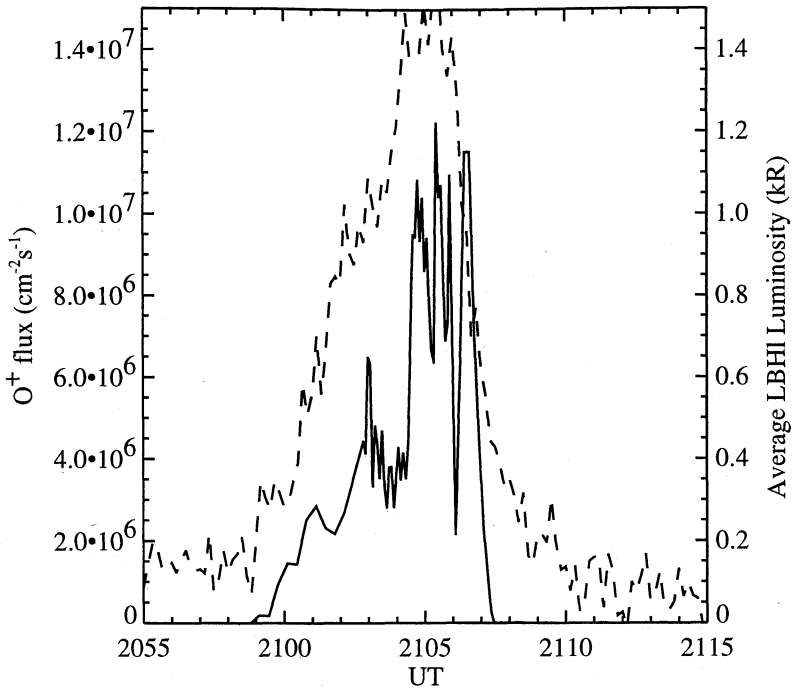


**Figure 1.** The $O^+$ escape flux (solid line) measured by the FAST/Time-of-Flight Energy Angle Mass Spectrometer (TEAMS) instrument on January 28, 1997, between 2055 and 2115 UT. Also plotted is the average (over six image frames) LBHl luminosity (dashed line) along the magnetic foot point of the satellite.

the activation region showed no significant $x$ deflection near 2100 UT.

Figure 1 shows the flux of escaping $O^+$ as a function of time measured by the TEAMS instrument on FAST. Also shown in Figure 1 is the average LBHl auroral intensity (moving foot point average over the closest image plus the previous five images, ~7.7-min window) along the satellite's magnetic ground track. Clearly, the fluxes are highest in that portion of the auroral zone where the intensification occurred even though the intensification appears to have subsided somewhat by the time FAST arrived on the field line that maps to that portion of the aurora (at 2104:47 and 2105:24 UT in Plate 1). As will become apparent in section 4, the flux of escaping $O^+$ does not correlate as well with the current level of auroral activity as it does with the level of activity in the recent past.

Our second example is from February 9, 1997, between 1920 and 1936 UT (Plate 2 and Figure 2). On this date the $F10.7$ index was again 71 ($\times 10^{-22}$ W m$^{-2}$ Hz$^{-1}$) and at the time of the pass the *Kp* index was 5+. For the 3-hour interval from 1800 to 2100 UT, *Dst* was decreasing from –25, to –49, to –54 nT. Thus a small magnetic storm was in progress, and at the time of the pass the ring current was growing in intensity. For this case then the conditions are wintertime, solar minimum, with a moderate to high level of magnetic activity.

In this event the FAST magnetic ground track passed over western Russia and out over the Arctic Ocean, just to the east of the ground track of the previous case. For many minutes prior to 1920 UT, auroral activity (as measured by the intensity of the UVI LBHl images) below the FAST ground track and to the west was low compared to that seen to the east of the ground track. Just as FAST approaches the auroral zone, activity spreads to the west as far as southern Greenland. During the following minutes, activity also spreads poleward along a broad front from Scandinavia to eastern Russia. The westward surge of auroral activity is seen in ground magnetometers as a negative deflection in the $x$ component of 165 nT at Oulujärvi (OUJ; 64.5°, 27.2°) at 1924 UT, 690 nT at Leirvogur (LRV; 64.2°, 338.3°) at 1925 UT, and 300 nT at Narsarsuaq (NAQ; 61.1°, 314.8°) at 1927 UT. The most intense aurora seen in this sequence of UVI images is over Leirvogur.

The $O^+$ escape flux measured by the TEAMS instrument between 1920 and 1936 UT is plotted in Figure 2 along with the averaged (~7.7-min window) LBHl auroral intensity along FAST's magnetic ground track. As FAST approaches the low-latitude side of the auroral zone, the $O^+$ escape flux gradually increases. About 90 s to 2 min after entering the region of very intense auroral electron precipitation the $O^+$ escape flux peaks above $2\times10^7$ cm$^{-2}$ s$^{-1}$ at 1925 UT. This is between the 1923:38 and 1926:42 UT images in Plate 2. Between 1926 and 1929 UT the $O^+$ escape flux drops to somewhat lower levels. Between 1930 and 1934 UT this flux increases to values near $10^7$ cm$^{-2}$ s$^{-1}$ when FAST flies over a portion of the auroral zone that has expanded poleward. By 1936 UT, FAST has passed poleward of the highest latitude portion of the aurora and the $O^+$ escape flux has dropped to very low levels. Again, one can see that the oxygen ion escape flux is closely tracking auroral activity with a possible delay of a few minutes.

## 4. Statistical Analysis

Because of the large number of passes available to analyze, we can do statistical analysis to better see the trends in the data. For our first attempt we use data from 19 nightside auroral zone FAST passes made between February 7 and 11, 1997. The orbit number, date, and time interval of the passes

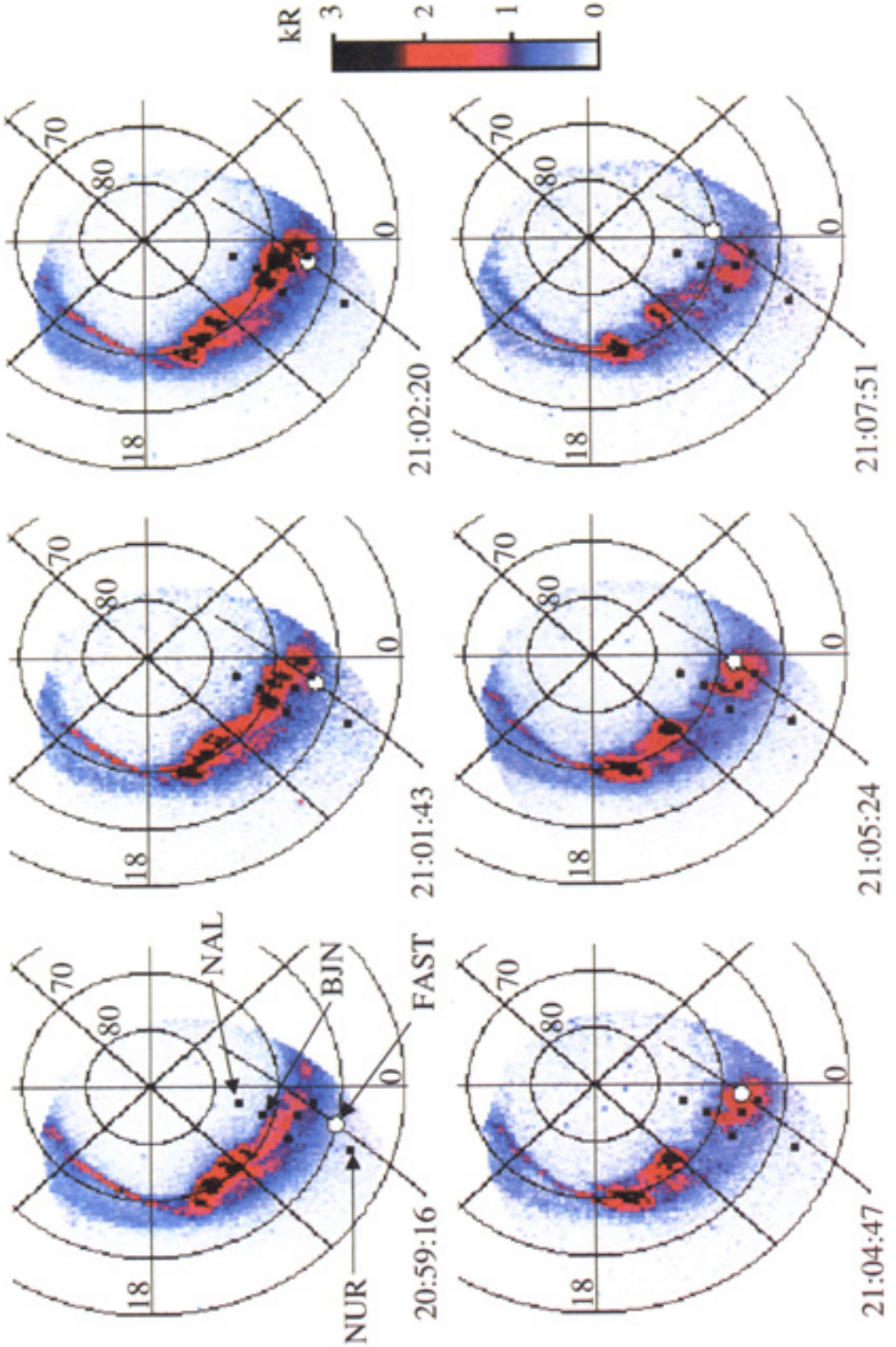


**Plate 1.** Six consecutive Ultraviolet Imager (UVI) Lyman-Birge-Hopfield-long (LBHl) images of the aurora taken on January 28, 1997, at the indicated times. Overlaid in these images is the position of the Fast Auroral Snapshot (FAST) spacecraft mapped along magnetic field lines to an altitude of 100 km. The small white circle indicates the position of FAST at the time of the image. The locations of several ground magnetometer stations are indicated by the small black squares. Those marked are Bear Island (BJN), Ny Ålesund (NAL), and Nurmijärvi (NUR).

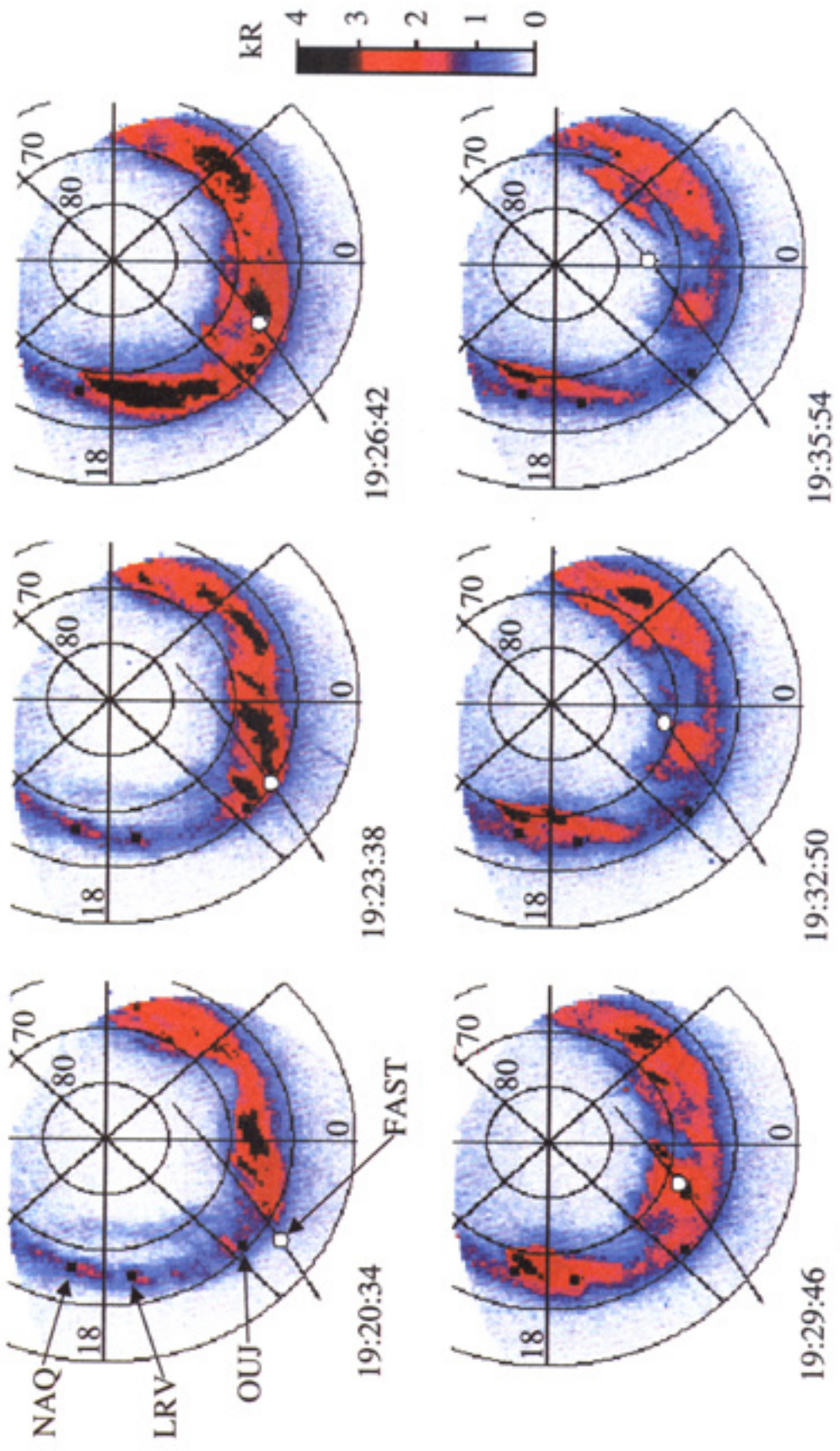


**Plate 2.** Same as Plate 1 except for the February 9, 1997, event.

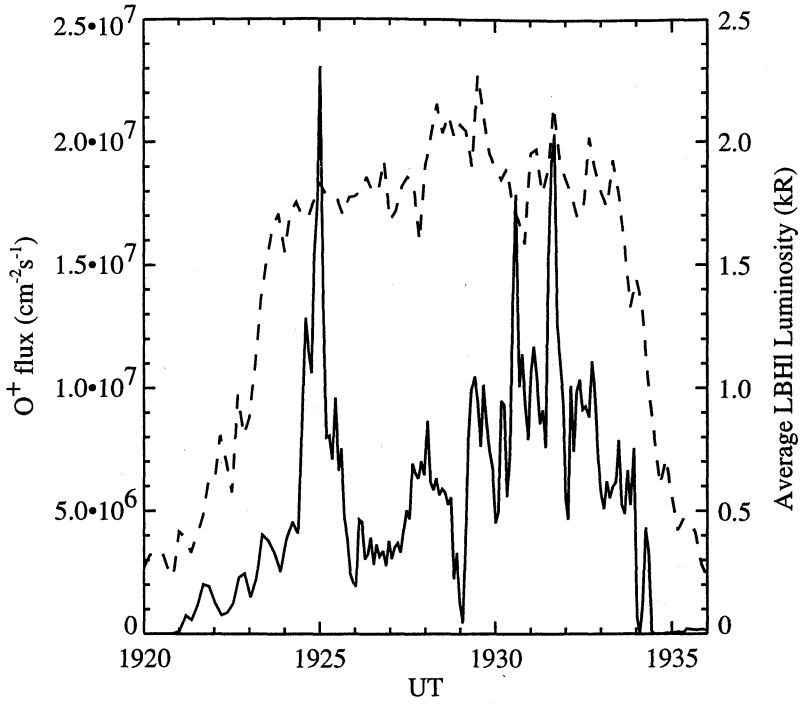


**Figure 2.** Same as Figure 1 except for the February 9, 1997, event.

are listed in Table 1. Also included in Table 1 is the value of the *Kp* index at the time of each pass. The time interval indicates that portion of the orbit from which the TEAMS instrument data were used. The appropriate interval to use was determined by a visual inspection of the UVI images, like those of Plates 1 and 2, for each pass. Among the 19 passes, we have 2232 samples of the $O^+$ escape flux. All of the passes occurred on the nightside with magnetic local times between 2000 and 0100.

In Figure 3a we plot the 2232 flux values versus the intensity (in kilorayleighs of the LBHl band) of the aurora at the foot point of the field line that the FAST spacecraft is on. In doing this we use the UVI image that is closest in time to the time of the flux measurement. In some cases this image was taken after the $O^+$ flux was measured. The average time difference between the flux measurement and the image is indicated by the value of *dt* to the right of the image. In this case this value is much smaller than 1 min.

**Table 1.** FAST[a] Orbits Used in the Statistical Analysis Presented in Figures 3 and 4.

| Pass | Orbit Number | Date | Universal Time | Kp |
|---|---|---|---|---|
| 1 | 1834 | Feb. 7, 1997 | 0040-0055 | 1+ |
| 2 | 1838 | Feb. 7, 1997 | 0936-0958 | 0+ |
| 3 | 1840 | Feb. 7, 1997 | 1410-1425 | 0+ |
| 4 | 1850 | Feb. 8, 1997 | 1217-1235 | 3+ |
| 5 | 1861 | Feb. 9, 1997 | 1245-1300 | 3+ |
| 6 | 1862 | Feb. 9, 1997 | 1453-1517 | 4 |
| 7 | 1863 | Feb. 9, 1997 | 1709-1722 | 4 |
| 8 | 1864 | Feb. 9, 1997 | 1920-1935 | 5+ |
| 9 | 1865 | Feb. 9, 1997 | 2130-2153 | 4 |
| 10 | 1870 | Feb. 10, 1997 | 0840-0858 | 4 |
| 11 | 1872 | Feb. 10, 1997 | 1309-1328 | 3+ |
| 12 | 1873 | Feb. 10, 1997 | 1522-1536 | 3+ |
| 13 | 1874 | Feb. 10, 1997 | 1734-1751 | 3+ |
| 14 | 1878 | Feb. 11, 1997 | 0224-0240 | 3 |
| 15 | 1880 | Feb. 11, 1997 | 0647-0713 | 4 |
| 16 | 1881 | Feb. 11, 1997 | 0904-0925 | 4- |
| 17 | 1882 | Feb. 11, 1997 | 1115-1140 | 4- |
| 18 | 1885 | Feb. 11, 1997 | 1801-1817 | 3+ |
| 19 | 1886 | Feb. 11, 1997 | 2010-2030 | 3+ |

[a]FAST, Fast Auroral Snapshot

Clearly, the trend in the data is for the flux to increase with increasing auroral intensity. To describe this trend we fit the data, using the least squares method, with the following function:

$$\log_{10} F(O^+) = A\,[1 - \exp(-a\,x)] + B, \qquad (1)$$

where $x$ is the LBHl auroral luminosity in kilorayleighs, $A$, $a$, and $B$ are fitting parameters, and the flux is given in units of ions $cm^{-2}\ s^{-1}$. The value of these three parameters for the data in Figure 3a are $A = 2.12$, $a = 1.57$, and $B = 4.55$. At zero luminosity the $O^+$ escape flux is then $3.6\times10^4$ $cm^{-2}\ s^{-1}$ and at a luminosity of 4 kR it is $4.6\times10^6$ $cm^{-2}\ s^{-1}$. For this range in luminosity the $O^+$ escape flux increases by a factor of 130. The values of the fitting parameters are also listed to the right of the plot in Figure 3a. Beneath those are the percent fitting error ($Err=100\{\Sigma[1-y_i/y(x_i)]^2/N\}^{1/2}$; $y_i$ is the measured oxygen flux, $y(x_i)$ is the calculated flux from (1), and the sum is over all data points $N$) and the correlation coefficient (CC) between the fluxes and luminosities.

To investigate the effect of auroral activity from the recent past on the relationship between fluxes and luminosities, we plot in Figure 3b the same 2232 flux data points, now versus the average luminosity at the foot point of the field line. For the averaging we use the image closest in time to the flux measurement plus the previous three images. Four image frames are then averaged to give the ordinate value. The value of *dt* in this case is now 4.6 min, meaning that the average time interval into the past of the fourth image frame is 4.6 min. By doing this, the correlation coefficient has increased from 0.56 to 0.65, and the percent fitting error has been

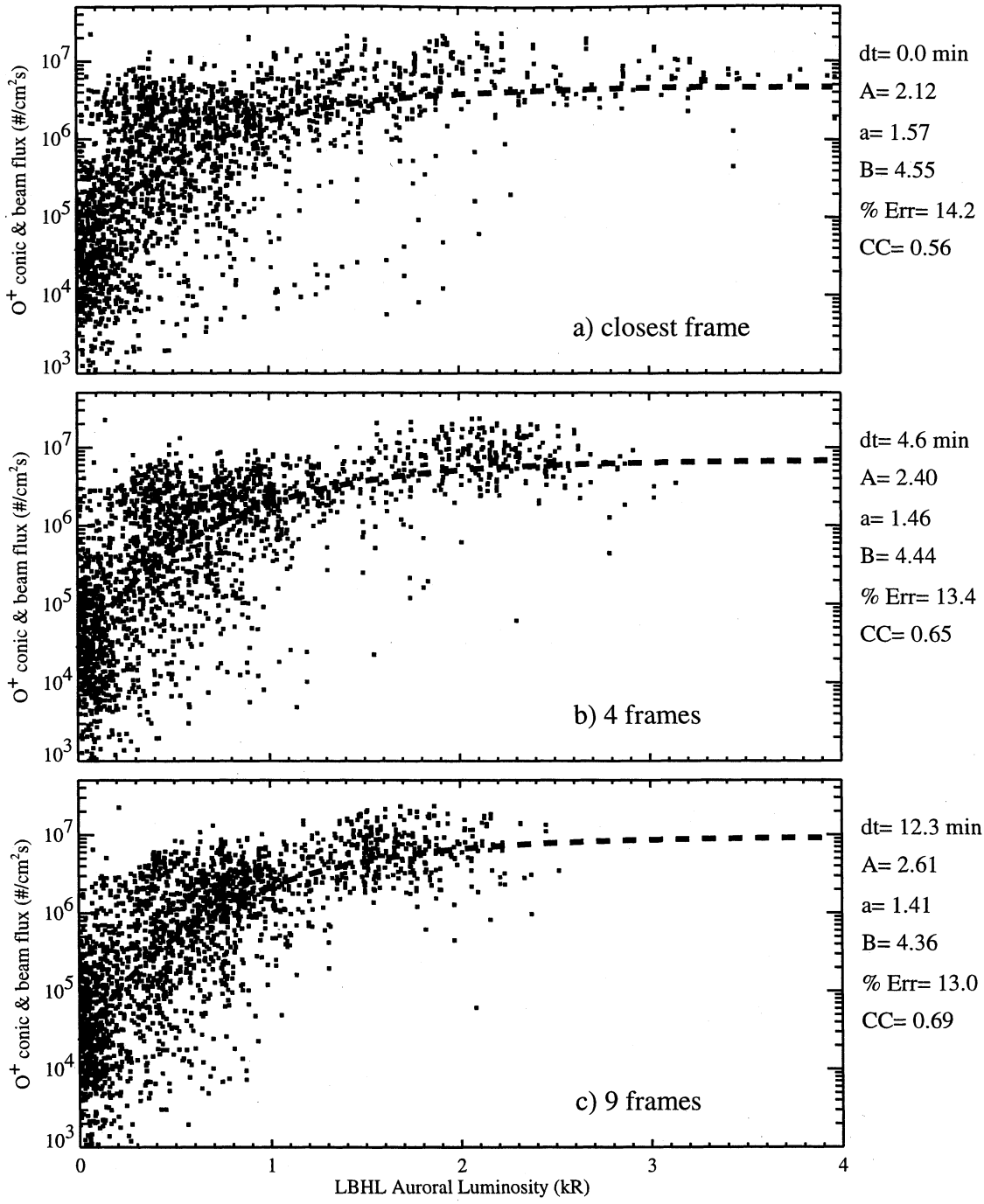


**Figure 3.** Plots of individual $O^+$ escape flux measurements versus LBHl auroral luminosity at the foot point of the field line. (a) The luminosity of the image frame closest in time to the flux measurement. (b) The average luminosity of the closest image frame plus the previous three frames. (c) The average luminosity of the closest plus the previous eight image frames. The numbers to the right of each panel indicate the average time interval into the past over which the images were averaged, the three parameters of the fitting function (*A, a,* and *B*), the percent error of that fit, and the correlation coefficient.

reduced from 14.2 to 13.4. In addition, the fitting parameter *A* has increased from 2.12 to 2.40, and *B* has decreased slightly from 4.55 to 4.44. In this case an increase of the average foot point luminosity from 0 to 4 kR results in an increase in the $O^+$ escape flux by a factor of 250.

If we average nine image frames into the past, we get the results in Figure 3c. Here we have used auroral luminosities that extend, on average, 12.3 min into the past. By doing this, the correlation coefficient increases to 0.69. The value of *A* increases to 2.61, and *B* decreases slightly to 4.36. Here a 0–4 kR increase in the average foot point luminosity gives an increase in the $O^+$ escape flux by a factor of 400.

On the surface it appears that the addition of information from the recent past improves the correlation between oxygen flux and auroral luminosity, but there is something else going on here as well. It is known that small-scale structures exist in the aurora at spatial scales below the resolution of the UVI. Short-timescale fluctuations in these small-scale features can

cause individual UVI pixels to fluctuate in intensity introducing a type of "random noise." Time averaging of a sequence of images would reduce this "noise" and give for each pixel a closer representation of its average value. Any actual correlation between the values of individual pixel luminosities and some other quantity would be more readily revealed by such an averaging process. So the results in Figures 3b and 3c show an improved correlation coefficient because of time averaging adding information from the recent past and reducing the effect of small-scale fluctuations. At the moment we cannot tell which of the two processes dominates.

In Figure 4 we repeat the exercise of Figure 3, only in this case instead of plotting the $O^+$ escape fluxes versus average LBHl foot point luminosity we plot it versus the luminosity of individual frames from the past. Thus, in Figure 4a the escape fluxes are plotted versus the luminosity of the image frame closest in time. This panel duplicates Figure 3a. In Figure 4b we plot oxygen fluxes versus the foot point luminosity for the fourth image frame back in time, and for Figure 4c we plot these fluxes versus the ninth image frame back.

Figure 5a tracks the correlation coefficient for these two different ways of including past information into the correlation, time averaging, or single frames. The solid line is for the time-averaging case while the dashed line is for the single-frame case. Initially the two curves follow each other, but after 4 min they separate with the single-frame correlation

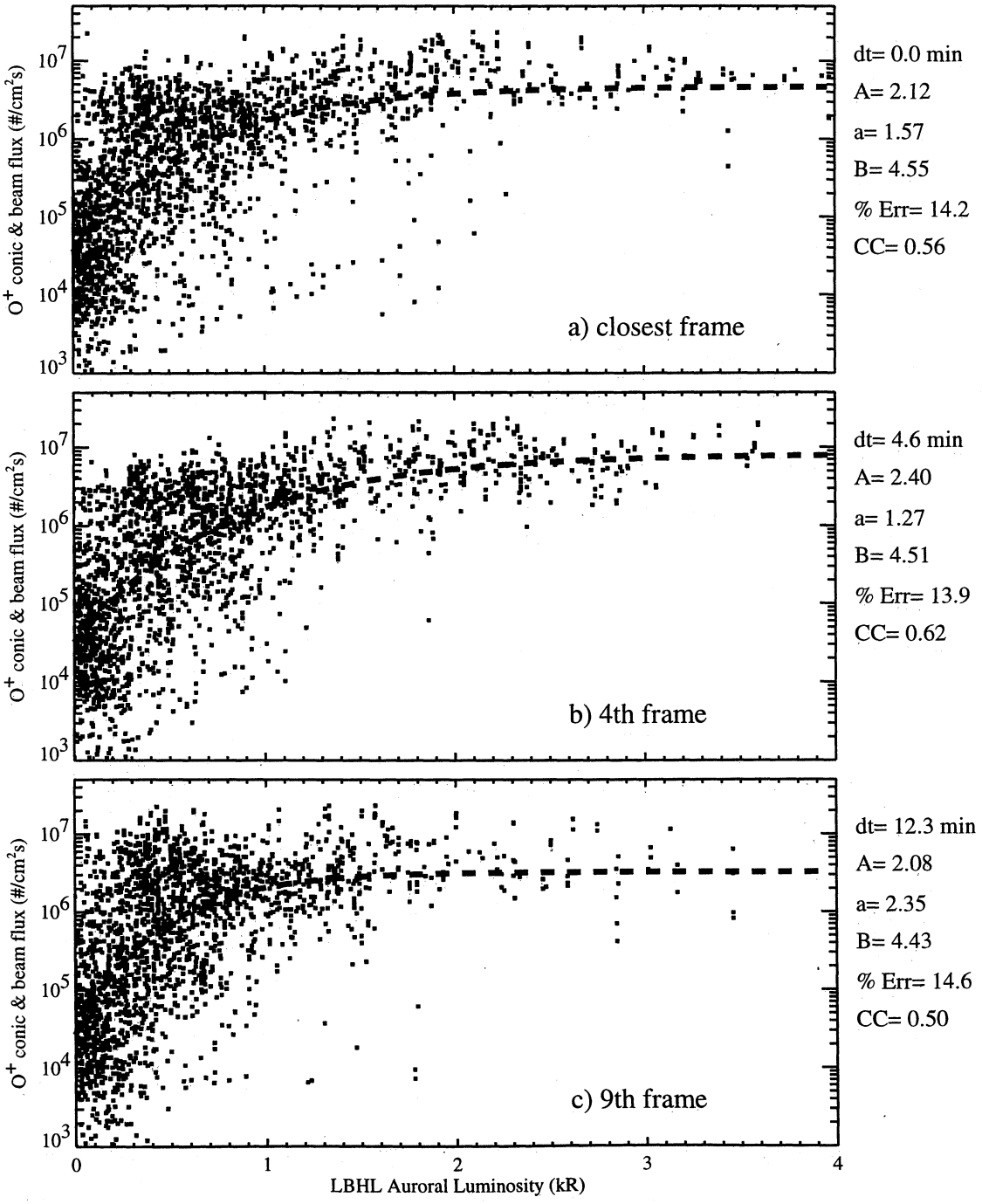


**Figure 4.** (a-c) Same as Figure 3 except that the fluxes are plotted against the luminosity from the given image frame in the past and not against the average luminosity.

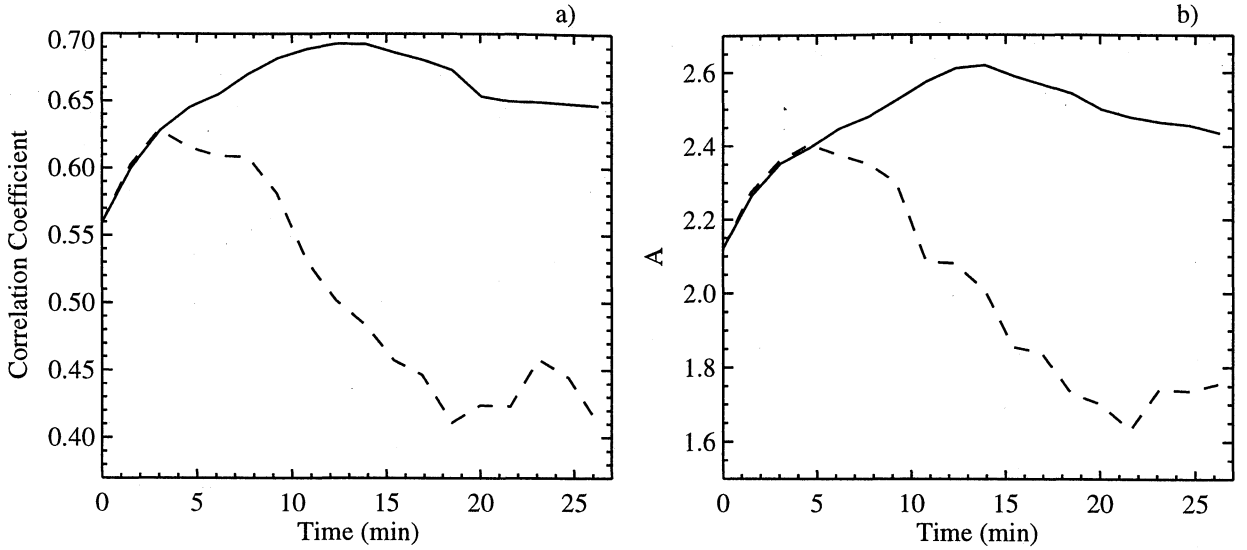


**Figure 5.** (a) Plot of the correlation coefficient for a series of cases like those in Figure 3 (solid line) for images averaged over the indicated time into the past, and those in Figure 4 (dashed line) for images at the indicated times in the past. (b) Plot of the fitting parameter $A$ from equation (1) for the same cases as in Figures 3 and 4.

coefficient dropping to ~0.4 after 20 min. The time-averaging correlation coefficient peaks after 12 min and declines thereafter. Figure 5b shows the value of the fitting parameter $A$ from (1) for each case. These values follow the same trend as that for the correlation coefficient as might be expected.

The results in Figure 5 show that the highest correlation between $O^+$ escape flux and foot point LBHl auroral luminosity is achieved when luminosities from 5 to 12 min in the past are used in place of (or with) concurrent luminosities or luminosities from much further in the past. The result of this exercise suggests that the magnitude of the $O^+$ escape flux out of the nightside auroral zone, seen between 3000- and 4000-km altitude, is determined by the energy input into the ionosphere that occurred between 5 and 12 min in the past. This delay may represent nothing more than the travel time for the lowest-energy (~10 eV) ions to travel from the topside ionosphere (500 km) to the satellite altitude (see Table 2).

As a further test of this result, in Figure 6 we repeat the exercise of Figure 3 and 4 using a different data set. Here we use 31 FAST passes that occurred between the dates of January 25 and 31, 1997. In total there are 31 passes with 3060 data points. Although the correlation coefficients are lower and the fitting error is higher here (because of the larger number of data points), the same trend is evident. When time averaging auroral luminosities, the best correlation occurs after averaging for 11 min into the past. When using individual image frames the highest correlation occurs at ~2 min in the past. For this case the $O^+$ flux in the 3000- to 4000-km altitude range seems to be determined by foot point auroral conditions between 2 and 11 min in the past.

In our analysis of the TEAMS data we looked at the number flux and energy flux of escaping suprathermal $O^+$ and $H^+$ ions. We found that the best correlations were for the $O^+$ number flux, and hence decided to focus our efforts on that quantity. Being the slowest ion of the three main ions observed by TEAMS ($H^+$, $He^+$, and $O^+$), $O^+$ should exaggerate any time delays and make them more apparent.

**Table 2.** Oxygen Ion Flight Times[a] (s)

| | Energy, eV | | |
|---|---|---|---|
| Pitch Angle, deg | 10 | 32 | 100 |
| | | 500–4000 km | |
| 100 | 658 | 316 | 171 |
| 140 | 416 | 212 | 116 |
| 180 | 354 | 185 | 102 |
| | | 1000–3000 km | |
| 100 | 435 | 217 | 118 |
| 140 | 234 | 125 | 69 |
| 180 | 193 | 104 | 58 |

[a]The effects of gravity and the mirror force are included in the calculation while the effects of any parallel electric fields, or additional ion heating are ignored.

## 5. Scatter in the Data

In an ideal world the $O^+$ flux values when plotted versus LBHl luminosities would fall along a smooth narrow line, assuming that there was a relationship between the two. In the real world, scatter in the data is inevitable. Why is there so much scatter in the data plotted in Figures 3, 4, and 6? (Is it an indication of variable energy partitioning or something else?) The reasons can be classified as due to instrumental effects, operational effects, and geophysical effects. Both instruments involved in this study, the TEAMS instrument and the UVI, have their intrinsic errors that give variability to the results. The lack of a correction for ram and spacecraft potential effects means that some, as yet unquantified, variability exists in the TEAMS instrument $O^+$ escape fluxes. In addition, there is a spatial resolution difference between the two instruments. During the time interval when an image is accumulated, the UVI samples a region in the ionosphere that is 30 by 300 km. During the 5 s that the TEAMS instrument takes to obtain a sample, it covers a region that is a few meters wide by 20–30 km long. Depending on the degree to which small-scale structures exist, the two may be looking at entirely different situations.

Since the UVI was operating in a mode where it took two LBHl images followed by two LBHs images, the sequence of

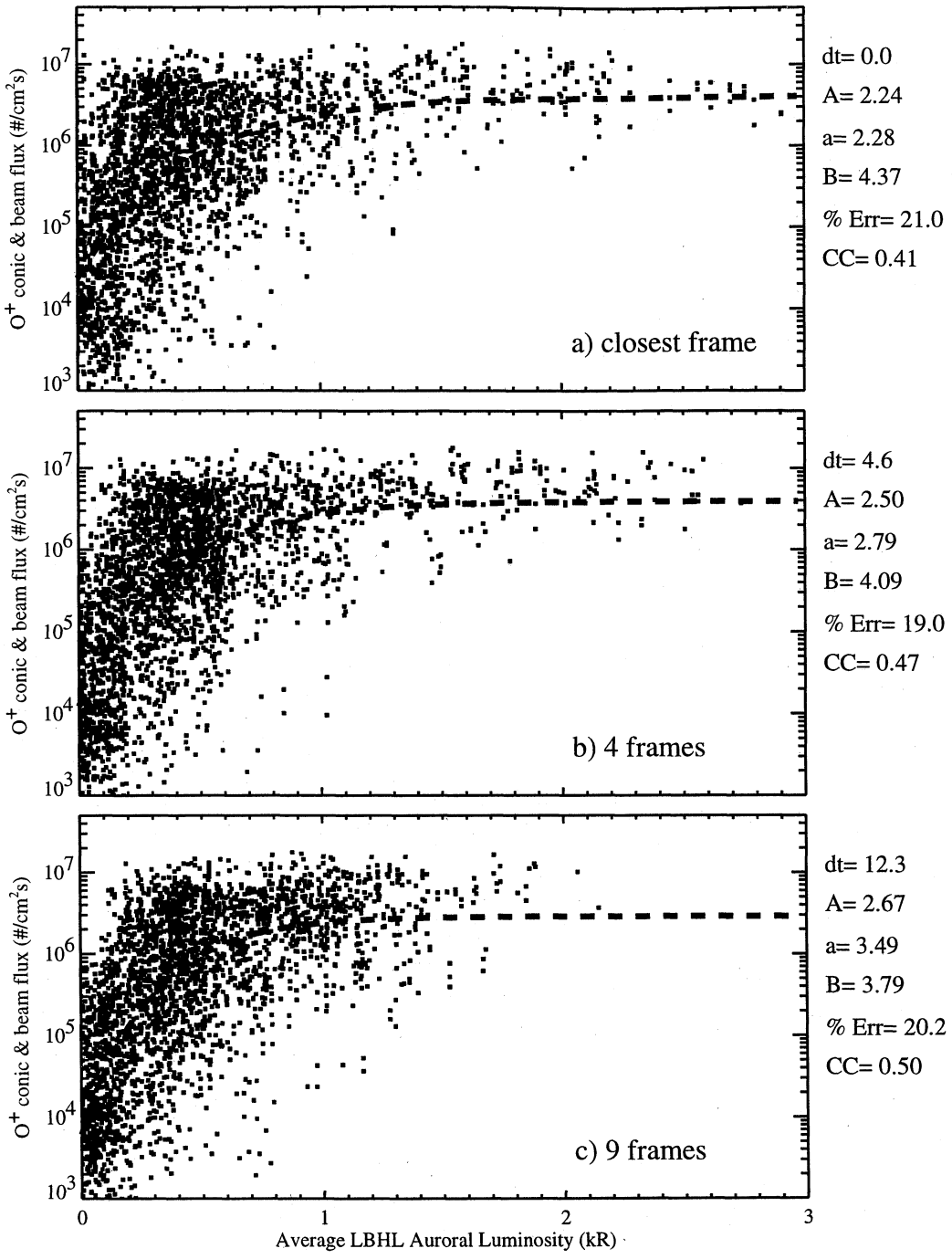


**Figure 6.** Same as Figure 3 except applied to the data from January 25-31, 1997.

images used in our study has periodic 2-min gaps. When the aurora is very active and the precipitating electron energy flux is intense, it is often highly time variable. The gaps in the UVI image sequences mean that it is possible that a given sequence will not represent the actual variations in the aurora. Because of this, when the integrated emissions are found, it will be less than the true value. When the time-averaged emissions are found, it will be larger or smaller than the true value, depending on whether the aurora was brighter or dimmer during the gaps.

The geophysical reasons for the data scatter include variability in the characteristics of the underlying ionosphere and thermosphere, which will affect the amount of $O^+$ available for energization and outflow and possibly the altitude at which the wave-heating process will occur. The last possible geophysical reason for data scatter is related to the fact that low-energy precipitating electrons deposit most of their energy at high altitudes and do not produce much in the way of LBH emissions. For such electrons there will be little for the UVI to see in the LBHl and LBHs bands.

Among the FAST passes assembled for the February 7-11 data set there were four in which the TEAMS instrument measured $O^+$ suprathermal escape flux was quite high ($10^6$ – $10^7$ $cm^{-2}$ $s^{-1}$) but for which the UVI LBHl images showed

nothing. Time averaging of the image sequences for these passes gave values for the LBHl emissions along the satellite's magnetic ground track that were consistent with zero, meaning that individual pixel fluctuations had a mean of zero. These four passes were not used in the data set for Figures 3 and 4. Examination of measurements of precipitating electrons made by the electrostatic analyzer (ESA) on FAST showed that there were indeed precipitating energetic electrons in the region of ion outflow, but their mean energy was below 1 keV.

Examination of the scatterplots in Figures 3 and 4 shows that there is more scatter at low auroral luminosities than there is at high luminosities. When the four passes mentioned above are added to this data set the low-luminosity scatter increases. For example, the correlation coefficient for Figure 3a) went from 0.56 to 0.54, and for Figure 3c) it went from 0.69 to 0.64. This experience suggests to us that some of the remaining scatter could be accounted for by the presence of low-energy precipitating electrons in passes that were included in the data set.

## 6. Discussion

From the results of the previous sections it is clear that there is a relationship between the auroral luminosity in the 1600–1800 Å band and the escape flux of suprathermal $O^+$ ions. Why should this relationship exist? The intensity of the emissions in the LBHl band is proportional to the energy flux of the precipitating electrons. Auroral electron energy fluxes derived from the UVI LBHl images were compared to in situ satellite data [*Germany et al.*, 1997] and ground-based radar data [*Doe et al.*, 1997], and it was found that the UVI-derived electron energy fluxes agreed well with those obtained by the other two methods. The close correspondence between the intensity of the LBHl images and the energy flux of the precipitating auroral electrons suggests that the $O^+$ escape flux is a function of the precipitating electron energy flux or a closely related quantity.

The near-Earth space above the auroral zone is a region of energy convergence and dissipation. The recent results of *Wygant et al.* [2000] suggest that the aurora is powered by earthward directed Alfvén waves which dissipate much of their energy in the auroral acceleration region heating electrons. These energetic electrons then precipitate into the lower atmosphere producing the visible aurora. The suprathermal ions observed by TEAMS are heated in the region between the auroral acceleration region and the *F*2 peak in the ionosphere. As such, they represent one channel by which the energy leaving the acceleration region toward the Earth is dissipated. Atmospheric emission of UV photons is another. Our results suggest that at least as far as these two processes are concerned, the fraction of the precipitating energy flux that is partitioned between them remains relatively constant as this flux increases or decreases.

This raises some interesting questions. Since the upward energy flux carried by the escaping suprathermal ions is small compared to the energy carried by the precipitating electrons, only a small fraction of the energy leaving the auroral acceleration region is partitioned into ion heating. If this fraction is highly variable, it could mask any correlation between ion escape fluxes and auroral luminosities. Our results suggest that this fraction is stable, but why? Does the structure of the thermosphere, the structure of the ionosphere, or the characteristics of the precipitating electrons determine this partitioning? Another complication to this whole situation is the fact that at least some of the escaping suprathermal $O^+$ ions are produced by impact ionization of atomic oxygen by the precipitating electrons themselves. Does this affect or even control the saturation flux of escaping $O^+$ ions seen in the data? These questions may be answered by self-consistent modeling.

One possible interpretation of our results is that the auroral electrons themselves are directly responsible for the elevated number fluxes of suprathermal $O^+$ ions. These electrons can affect the outflow of $O^+$ ions by (1) increasing their production rate through impact ionization, (2) increasing the topside $O^+$ scale height through heating of the thermal electrons, and (3) directly energizing the ions through joule heating. However, it is unlikely that these processes will produce the requisite ion energies above 10 eV. The most common type of ion energization process in the 1000- to 4000-km altitude region involves BBELF waves [*André et al.*, 1998; *Lund et al.*, 2000], which are not associated (on small scales) with precipitating auroral electrons. They are instead associated with suprathermal electron bursts, precipitating electrons with mean energies less than 1 keV.

Another possible interpretation is that auroral electrons are not directly responsible for ion energization but, nevertheless, set up the conditions so that energization will occur nearby. One way this could be done is through field-aligned currents and current continuity. Since precipitating auroral electrons either represent or are associated with a current out of the ionosphere, somewhere nearby there must be a return current to the ionosphere, set up at the same time, where the energization could occur. If this is true, then the positive correlation in our results suggests that the heating process on the return current field lines is controlled by the energy carried by the precipitating electrons. It also suggests that there is often fine-scale structure, with regions of alternating field-aligned currents closely spaced, on a scale below the resolution of the UVI images.

The statistical studies of *André et al.* [1998] and *Lund et al.* [2000] point out the fairly common occurrence of ion heating by electromagnetic ion cyclotron (EMIC) waves, at least in the premidnight MLT sector where they may be as common as BBELF events. EMIC waves are associated with precipitating auroral electrons. Since all of our data come from the premidnight to midnight MLT sector, it is possible that some of our events involve $O^+$ energization by EMIC waves.

Since the number flux is typically dominated by the lowest-energy particles, the time delay that we see in our results between auroral intensification and $O^+$ flux increases at 3000- to 4000-km altitude could be nothing more than the travel time for 10-eV ions to go from the topside ionosphere (~500 km) to the altitude of FAST. Table 2 lists travel times for a variety of different initial conditions and travel distances. For 10 eV $O^+$ ions this time ranges from ~3 min to ~11 min, depending on distance traveled and initial pitch angle. The energization process must quickly begin heating $O^+$ ions in the topside ionosphere to $\geq$ 10 eV; there is no indication of a more leisurely multistep process.

## 7. Conclusions

In listing the conclusions of this paper it should be kept in mind that they apply to the nightside auroral zone ionosphere

during wintertime, solar minimum conditions. Our three main conclusions are then the following:

1. The location of suprathermal ion outflow closely tracks the local aurora (as seen in the 1600–1800 Å band), regardless of how convoluted the auroral forms may be. That is, where there is aurora, there will be suprathermal $O^+$ outflow. The reverse is not always true. In several cases mentioned in the text, significant suprathermal ion outflow was seen in the absence of LBHl auroral forms.

2. For increases in auroral luminosity in the 1600–1800 Å band, from 0 to 4 kR, the $O^+$ escape flux increases by over 2 orders of magnitude. This can readily be seen in Figure 3, 4, and 6 where the average value of the fitting parameter $A$ (= $\log_{10}$ $[F_{O+}(x=\infty) - F_{O+}(x=0)]$) where $x$ is the LBHl luminosity in kilorayleighs) is 2.4.

3. The time delay between auroral brightening and saturation $O^+$ flux reaching 4000-km altitude is 5–10 min. This is established by several means. First, averaging the foot point auroral luminosity for 5–10 min into the past better organizes the relationship between the $O^+$ escape flux and the luminosity. Second, in a number of cases (two of which are illustrated in section 3 of this paper) the most intense fluxes of escaping $O^+$ are seen over aurora that has intensified within the previous 5–10 min.

**Acknowledgments.** We express our thanks to the FAST and Polar project teams for making these missions possible and to the UVI and TEAMS engineers and technical staff for making the data sets readily available and easily useable. FAST mission operations are supported by National Aeronautics and Space Administration grant NAS5-31283 to the University of California at Berkeley. We thank the Finnish, German, Norwegian, Polish, Russian, and Swedish institutes which maintain the IMAGE magnetometer array. Data from the Andenes, Bear Island, Kevo, Lovozero, Nurmijärvi, Ny Ålesund, and Oulujärvi stations were provided by the Finnish Meteorological Institute. Magnetometer data from the Leirvogur and Narssarssuaq stations were provided by the World Data Center-C2 for Geomagnetism in Kyoto, Japan. This work was funded by the NASA International Solar-Terrestrial Physics (ISTP) guest investigator program through contract NASW-99002 to Mission Research Corporation in Nashua, New Hampshire.

Janet G. Luhmann thanks William K. Peterson and Andrew W. Yau for their assistance in evaluating this paper.

## References

André, M., and A. Yau, Theories and observations of ion energization and outflow in the high latitude magnetosphere, *Space Sci. Rev., 80*, 27, 1997.

André, M., P. Norqvist, L. Andersson, L. Eliasson, A. I. Eriksson, L. Blomberg, R. E. Erlandson, and J. Waldemark, Ion energization mechanisms at 1700 km in the auroral region, *J. Geophys.Res., 103*, 4199, 1998.

Daglis, I. A., S. Livi, E. T. Sarris, and B. Wilken, Energy density of ionospheric and solar wind origin ions in the near-Earth magnetotail during substorms, *J. Geophys. Res., 99*, 5691, 1994.

Doe, R. A., J. D. Kelly, D. Lummerzheim, G. K. Parks, M. J. Brittnacher, G. A. Germany, and J. Spann, Initial comparison of Polar UVI and Sondrestrom IS radar estimates for auroral electron energy flux, *Geophys. Res. Lett., 24*, 999, 1997.

Germany, G. A., G. K. Parks, M. J. Brittnacher, J. Cummock, D. Lummerzheim, J. F. Spann, L. Chen, P. G. Richards, and F. J. Rich, Remote determination of auroral energy characteristics during substorm activity, *Geophys. Res. Lett., 24*, 995, 1997.

Giles, B. L., C. R. Chappell, T. E. Moore, R. H. Comfort, and J. H. Waite Jr., Statistical survey of pitch angle distributions in core (0–50 eV) ions from Dynamics Explorer 1: Outflow in the auroral zone, polar cap, and cusp,*J. Geophys. Res., 99*, 17,483, 1994.

Gorney, D. J., A. Clarke, D. Croley, J. F. Fennell, J. Luhmann, and P. Mizera, The distribution of ion beams and conics below 8000 km, *J. Geophys. Res., 86*, 83, 1981.

Hirahara, M., et al., Relationship of topside ionospheric ion outflows to auroral forms and precipitation, plasma waves, and convection observed by Polar, *J. Geophys. Res., 103*, 17,391, 1998.

Lund, E. J., et al., Transverse ion acceleration mechanisms in the aurora at solar minimum: Occurrence distributions, *J. Atmos. Sol.-Terr. Phys., 62*, 467, 2000.

Miyake, W., T. Mukai, and N. Kaya, On the origins of the upward shift of elevated (bimodal) ion conics in velocity space, *J. Geophys. Res., 101*, 26,961, 1996.

Möbius, E., et al., The 3D plasma distribution function analyzers with time-of-flight mass discrimination for Cluster, FAST, and Equator-S, in *Measurement Techniques in Space Plasmas: Particles*, Geophys. Monogr. Ser., vol. 102, edited by R. F. Pfaff, J. E. Borovsky, and D. T. Young,, p. 243, AGU, Washington, D.C., 1998.

Norqvist, P., M. André, and M. Tyrland, A statistical study of ion energization mechanisms in the auroral region,*J. Geophys. Res., 103*, 23,459, 1998.

Øieroset, M., M. Yamauchi, L. Liszka, S. P. Christon, and B. Hultqvist, A statistical study of ion beams and conics from the dayside ionosphere during different phases of a substorm, *J. Geophys. Res., 104*, 6987, 1999.

Peterson, W. K., A. W. Yau, and B. A. Whalen, Simultaneous observations of $H^+$ and $O^+$ ions at two altitudes by the Akebono and Dynamics Explorer 1 satellites, *J. Geophys.Res., 98*, 11,177, 1993.

Shelley, E. G., R. G. Johnson, and R. D. Sharp, Satellite observations of energetic heavy ions during a geomagnetic storm, *J. Geophys. Res., 77*, 6104, 1972.

Stevenson, B. A., J. L. Horwitz, G. A. Germany, P. D. Craven, T. E. Moore, B. L. Giles, G. K. Parks, and Y. J. Su, Relation of field aligned $O^+$ flows at 5000 km altitude to auroral structure and brightness, *Eos, Trans. AGU, 81*(19), Spring Meet. Suppl., SM51A-11, 2000.

Torr, M. R., et al., A far ultraviolet imager for the international solar-terrestrial physics mission, in *The Global Geospace Mission*, edited by C. T. Russell, p. 329, Kluwer Acad.,Norwell, Mass., 1995.

Viljanen, A., and L. Häkkinen, IMAGE magnetometer network, in *Satellite-Ground Based Coordination Sourcebook*, edited by M. Lockwood, M. N. Wild, and H.J. Opgenoorth, Eur. Space Agency Spec. Publ., *SP-1198*, 111, 1997.

Wilson, G. R., and P. Craven, Molecular ion upflow in the cleft ion fountain, *J. Geophys. Res., 104*, 4437, 1999.

Wygant, J. R., et al., Polar spacecraft based comparisons of intense electric fields and Poynting flux near and within the plasma sheet-tail lobe boundary to UVI images: An energy source for the aurora, *J. Geophys. Res., 105*, 18,675, 2000.

Yau, A. W., B. A. Whalen, W. K. Peterson, and E. G. Shelley, Distribution of upflowing ions in the high-altitude polar cap and auroral ionosphere, *J. Geophys. Res., 89*, 5507, 1984.

Yau, A. W., P. H. Beckwith, W. K. Peterson, and E. G. Shelley, Long-term (solar cycle) and seasonal variations of upflowing ionospheric ion events at DE 1 altitudes, *J. Geophys. Res., 90*, 6395, 1985a.

Yau, A. W., E. G. Shelley, W. K. Peterson, and L. Lenchyshyn, Energetic auroral and polar ion outflow at DE 1 altitudes: Magnitude, composition, magnetic activity dependence, and long-term variations, *J. Geophys. Res., 90*, 8417, 1985b.

Young, D. T., H. Balsiger, and J. Geiss, Correlations of magnetospheric ion composition with geomagnetic and solar activity, *J. Geophys. Res., 87*, 9077, 1982.

G. A. Germany, Center for Space Plasma and Aeronomic Research, University of Alabama in Huntsville, Huntsville, AL 35899.

E. J. Lund, Space Science Center, University of New Hampshire, Durham, NH 03824.

D. M. Ober and G. R. Wilson, Mission Research Corporation, 589 W. Hollis St., Nashua, NH 03062. (gwilson@mrcnh.com)

(Received November 21, 2000; revised February 6, 2001;
accepted February 6, 2001)